Measurement of Tool-Workpiece Interface Temperature Distribution in Friction Stir Welding

Axel Fehrenbacher
Department of Mechanical Engineering,
University of Wisconsin—Madison,
Madison, WI 53706

Joshua R. Schmale
Department of Mechanical Engineering,
University of Wisconsin—Madison,
Madison, WI 53706

Michael R. Zinn
Department of Mechanical Engineering,
University of Wisconsin—Madison,
Madison, WI 53706

Frank E. Pfefferkorn[1]
Department of Mechanical Engineering,
University of Wisconsin—Madison,
Madison, WI 53706
e-mail: pfefferk@engr.wisc.edu

The objective of this work is to develop an improved temperature measurement system for friction stir welding (FSW). FSW is a solid-state joining process enabling welds with excellent metallurgical and mechanical properties, as well as significant energy consumption and cost savings compared to traditional fusion welding processes. The measurement of temperatures during FSW is needed for process monitoring, heat transfer model verification and process control, but current methods have limitations due to their restricted spatial and temporal resolution. Previous work showed that temperatures at the tool shoulder-workpiece interface can be measured and utilized for closed-loop control of temperature. Adding an additional thermocouple at the tool pin-workpiece interface and performing a calibration of the measurement to gain better insight into the temperature distribution in the weld zone improved the method. Both thermocouples were placed in through holes right at the interface of tool so that the sheaths are in direct contact with the workpiece material. This measurement strategy reveals dynamic temperature variations at the shoulder and the pin within a single rotation of the tool in real-time. It was found that the highest temperatures are at the shoulder interface between the advancing side and the trailing edge of the tool, closer to the advancing side. The temperature distribution was mostly affected by travel speed and the temperature difference within one tool rotation was found to be between 10 °C and 50 °C, depending on the process parameters. The dynamic temperature measurements obtained with the current system are of unmatched resolution, fast, and reliable and are likely to be of interest for both fundamental studies and process control of FSW. [DOI: 10.1115/1.4026115]

Keywords: friction stir welding, temperature measurement, tool-workpiece interface, temperature distribution, aluminum

1 Introduction

FSW was invented at The Welding Institute in the United Kingdom in 1991 [1]. This relatively new, solid-state joining process differentiates itself from many other welding processes by not melting the workpiece. As a result, the joining process is energy efficient, environment friendly, versatile, and generates excellent joint properties.

The basic concept of FSW can be described as follows: a non-consumable rotating FSW tool with a specially designed shoulder and pin is pressed against the base metal surface, while a vertical downward force is applied (Fig. 1). Due to friction between the rotating tool and the workpiece (plastic deformation of the workpiece also produces heat), the temperature in the weld zone increases. The generated heat is usually not sufficient to melt the material, however, the workpiece is softened in the area around the pin and the deformation resistance (i.e., yield strength) of the base material decreases. The tool is traversed along the weld interface to mix the joining members in a forging action along the joining line to create a weld in the "solid state". Friction stir welding results in intense plastic deformation and temperature increase in the weld zone, which leads to a significant microstructural evolution without typically causing phase changes [2,3].

Friction stir welding was initially applied to aluminum alloys but welding of other materials such as copper, titanium, and magnesium alloys as well as steels and nickel alloys have been investigated [3]. Friction stir welding is also identified as a technology that can be used to join dissimilar alloys and metals. By maintaining the weld below the solidus temperature, minimal pre and post processing, excellent weld strength and ductility and environmentally friendly nature, the process enables cost reductions in many industrial applications and allows the joining of materials considered not weldable by fusion processes (e.g., highly alloyed 2XXX and 7XXX series aluminum). Friction stir welding has developed numerous potential applications in aerospace, automotive, railway, shipbuilding, construction, and other areas [2,3].

2 Motivation

Previous work showed that temperatures at the shoulder-workpiece (tool-workpiece) interface can be measured in real-time and can be utilized for closed-loop control of temperature [4,5]. The objective of this work is to develop an improved temperature measurement system to provide better insight into the FSW process, benefit the fundamental process understanding and ultimately help in maintaining and improving the weld quality by developing advanced closed-loop temperature control strategies. A sophisticated temperature measurement system can be valuable for general process monitoring, verifying thermal analytical and numerical models [6] and can provide feedback signals for process control [7].

Due to high instrumentation effort, relatively little work has been done in experimentally recording highly resolved weld

[1]Corresponding author.
Manuscript received September 10, 2012; final manuscript received November 20, 2013; published online January 16, 2014. Assoc. Editor: Robert Gao.

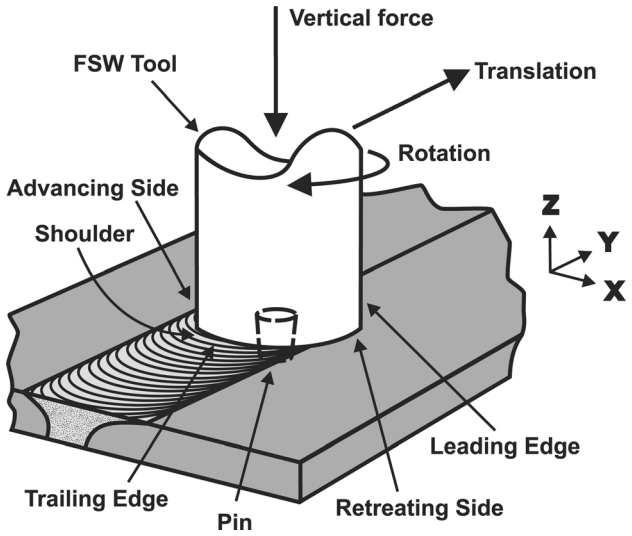

Fig. 1 Schematic of the FSW process

temperatures to gain insight into the actual process and to verify the simulation results from heat transfer simulations. Infrared thermography methods are used [8,9] but they only capture the surface temperatures of workpiece or tool and are associated with high uncertainties due to varying target emissivity, surface condition, etc. Typically, thermocouples are embedded in the workpiece or backing plate [10,11], away from the weld zone, but they only provide limited insight into the dynamics of the process due to their distance to the weld zone. Thermocouples have also been embedded into the path of the weld to obtain weld zone temperatures [12,13], but only up to the point when the tool welds over it and physically destroys the sensor. Methods that embed temperature sensors in the workpiece require high instrumentation effort for each weld, i.e., they cannot be reused on an unwelded workpiece. Alternatively, thermocouples have been inserted into the tool [14,15], greatly reducing the instrumentation effort per weld. All of the temperature measurement methods described are not able to provide measurements with sufficiently high temporal and spatial resolution to provide insight into weld dynamics.

Great effort has been made recently in developing numerical models of FSW with the goal to improve the understanding of the complex underlying physics of the process. Models have been developed that predict temperature distributions, material flow patterns, residual stresses, microstructure evolution, and others [16]. Temperature measurements used to verify such thermal models are typically lacking in the ability to provide temperatures close to the weld zone temperature (measuring workpiece surface temperatures or placing thermocouples too far away from the weld zone) or do not provide a high spatial resolution (limited number of thermocouples at fixed locations).

In addition to helping in the fundamental process understanding, the experimental knowledge of temperatures in FSW is of great interest because the weld zone temperature determines the microstructural evolution and the metallurgical and mechanical properties of the resulting weld. Previous studies have shown that the change in heat flow, hence weld temperature, had a measurable impact on the weld strength and residual stresses [17,18]. Relationships between temperature and weld quality have been reported in the literature for FSW: Peel et al. found that weld properties are dominated by the heat input (temperature) in welding aluminum 5083 [19]. Gratecap et al. found a qualitative influence of weld temperatures on weld quality [20]. Simar et al. observed effects of the weld heat input (by varying the travel speed) on the microstructure and the mechanical properties of the weld [21]. In order to correlate weld quality to temperature, it is important to measure temperatures as close as possible to the weld zone temperature.

Finally, in order to develop closed-loop temperature control algorithms, it is valuable to employ a temperature measurement technique that captures the dynamics of the process well and has a minimal time delay so that simpler controllers can be used. Longer delays (e.g., if thermocouples are placed further away from the weld zone) may lead to a necessary second (cascaded) power control loop [22].

3 Approach

Ideally, the temperature distribution in the weld zone is measured during FSW with a high spatial and temporal resolution. Because the temperature inside the weld (stir) zone cannot be measured directly in real-time without significant effort (e.g., using a neutron source [23]), another location, close to or on the boundary of the weld zone, must be measured.

Initial efforts were made to measure workpiece and tool surface temperatures using infrared radiography (single [17] and dual wavelength pyrometers, Table 1). To date, in experiments using aluminum alloys 5083-H111 and 6061-T6, repeatable measurements could not be achieved because other radiation sources (hot objects close to the target, i.e., the FSW tool) impact the temperature measurement through specular and diffuse reflection from the workpiece surface at the wavelengths that were investigated. The measurement is complicated by the low emissivity (high reflectivity) of as-received aluminum surfaces as well as the fact that the workpiece and tool surfaces near the weld zone have similar temperature magnitudes and large temperature gradients. It was concluded that the use of the single and dual wavelength pyrometers was not feasible under the conditions tested for the aluminum workpieces. It might however, be feasible to employ the pyrometers during welding of other materials with higher emissivities, e.g., oxidized steel or bronze castings.

An important result from a heat transfer model is that thermocouples placed close to the FSW tool shoulder result in significantly shorter time delays, shorter response times and are closer to the stir zone temperature than workpiece or tool surface temperature measurements with a pyrometer. Cederqvist et al. also reduced the time delay when measuring tool temperatures by placing thermocouples closer to the shoulder-workpiece interface [24]. Placing thermocouples very close to the tool-workpiece interface region is also of interest in metal cutting, where the recent development of micro thin film thermocouples embedded in the tool lead to greater insight of temperature transients at the tool-chip contact region [25]. In general, the FSW tool is made of a material (e.g., highly alloyed tool steel, H13) with a thermal diffusivity ($\alpha_{H13} = 6.8 \times 10^{-6}$ m^2/s at 350 °C) that is an order of magnitude smaller than the aluminum workpiece material ($\alpha_{6061\text{-}T6} = 7.2 \times 10^{-5}$ m^2/s at 477 °C). It is therefore desirable to place the thermocouples as close to the tool-workpiece interface as possible to minimize the time delay associated with heat flow through the tool. To the best of our knowledge, Gerlich et al. [26] were the first to insert thermocouples into through holes placed into a stationary FSW tool used for friction stir spot welding research. In this work, we are also making use of through holes to enable direct contact of the tip of the thermocouples with the workpiece material. We are employing the through hole strategy

Table 1 Key specifications of pyrometers used

	Single wavelength pyrometer	Dual wavelength pyrometer
Emissivity	Fixed at 0.95	Variable
Spectral response	8–14 μm	2.025–2.223 μm and 2.225–2.451 μm
Temperature range	−40–500 °C	200–600 °C
Model	Williamson Transtemp 290	Williamson PRO 92-20

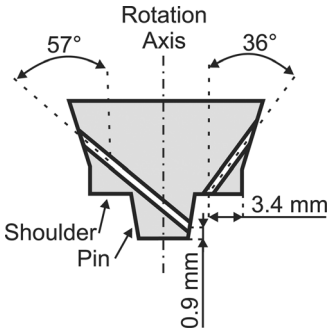

Fig. 2 Schematic of through hole locations for the thermocouples on the FSW tool (not to scale, section view). The thermocouples are exposed at the tool-workpiece interface.

for temperature measurements to reduce the dissipation delay during friction stir seam welding. The thermocouple assemblies are in direct contact with the surface of the workpiece material: in these tests an aluminum alloy that has a relatively high thermal diffusivity. Two 0.8-mm-diameter through holes were fabricated (using electrical discharge machining) into the tool shank (Fig. 2). One 7.5-mm-deep hole exits on the shoulder, 3.4 mm from the outer edge of the shoulder. Another, 14-mm-deep hole was made that exits on the side of the pin (location of a flat; see Fig. 5), 0.9 mm from the bottom of the pin, in order to obtain temperatures further down in the weld. The two through holes are placed in the same plane and the holes exit both on the same side of the rotation axis, i.e., they are located at the same angular position. The placement of the through holes was chosen to yield representative temperature data from both the shoulder and the pin location. A finite element method model (not discussed in this work) helped in choosing the locations as indicated in Fig. 2 with the goal of obtaining temperatures as close as possible to the weld zone temperature, minimizing the thermal delay as well as the response time.

A 0.25-mm-diameter (O.D. of sheath), sheathed, ungrounded, type K thermocouple was chosen to reduce the temperature response time (part no. TJ36-CAXL-010U by Omega Corp.). The two thermocouples were inserted into the through holes and secured with high temperature thermocouple cement (maximum service temperature 1426 °C). The thermocouple sheaths are in direct contact with the workpiece material during welding (no thermocouple cement between tip of thermocouple assembly and workpiece material).

In order to correlate the temperature measurements with the angular position of the FSW tool, a magnetically operated proximity sensor (Hall effect sensor, model 55140 by Hamlin) is used. A Hall effect sensor is a solid-state device with no moving parts and triggers when a magnetic field is nearby. The sensor chosen has a high enough switching speed (10 kHz) and is mounted on the rotating tool holder rather than stationary in order to synchronize the temperature measurements with the signal from the Hall effect sensor. One small magnet is mounted stationary ahead of the tool holder. Compared to rotary encoders, this method has a very limited resolution (only one pulse per tool revolution), but was considered to be sufficient for the given application.

Since the tool is rotating at high speed, a wireless data transmission system is used to transmit the temperature measurements in real-time (i.e., without significant delays) to a stationary data acquisition (DAQ) and control system. Figure 3 provides a schematic of the overall wireless DAQ system, illustrating the main components. Key specifications about the wireless instrumented tool holder are summarized in Table 2, more detailed information can be found in Ref. [5]. Figures 4 and 5 show a photograph of the instrumented tool holder and a close-up view of the FSW tool with the embedded thermocouples, respectively.

The measurement of real-time tool-workpiece interface temperatures by the tool-embedded thermocouple method should provide a unique insight into the physical processes governing the FSW

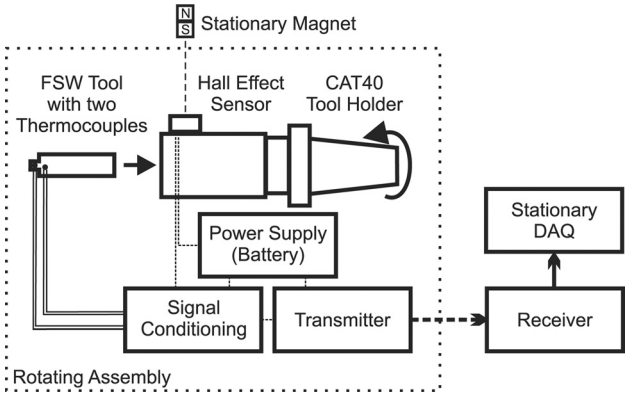

Fig. 3 Schematic illustrating the main components of the wireless DAQ system used for FSW

process. However, the temperature measured by the thermocouple is not equal to the tool-workpiece interface temperature. The difference in the measured temperatures from the interface temperatures is due to the dynamic response of the thermocouples: i.e., the thermocouple bead is actually located between 100 and 250 μm from the tool-workpiece interface. A modified laser flash method was developed to measure the dynamic response of the embedded thermocouples used in this work and calculate the true amplitude and phase of the tool-workpiece interface temperatures. When reporting temperatures in this work, both measured (at the thermocouple bead) and (corrected, i.e., true) interface are shown.

The method to calibrate the temperature measurements is based on the ASTM E-1461 standard to measure the thermal diffusivity of a substance. The thermocouples embedded into the tool were subjected to very short pulses of heat flux provided by a fiber laser. A photodiode was sampled by an oscilloscope and triggered the acquisition of temperature measurements. The thermal response of the thermocouples was recorded with respect to the applied heat flux and diffusive time constants were determined that govern the transport of thermal energy into a semi-infinite body. Those response times as reported in Table 2 are used in this work to calculate the true interface temperatures from the measured values.

Table 2 Key specifications of instrumented tool holder

Thermocouples	
Outer sheath diameter	0.25 mm
Sheath material	Super OMEGACLAD® XL
Calibration type	K
Junction type	Electrically insulated (ungrounded)
Response time calibrated while embedded in tool	Shoulder: 11 ms Pin: 37 ms
Upper temperature recommendation	600 °C (manufacturer provided)
Signal conditioning	
Amplifier gain	6.67 V/°C
Amplifier bandwidth	15 kHz
Amplifier calibration error	±1 °C
Amplifier temperature range	0–700 °C
A/D resolution	16 bit (0.01 °C)
A/D sampling frequency	5 kHz per channel
Angular position measurement	
Pulses per revolution	1
Switching speed	10 kHz
Wireless transmission	
Transmission frequency	250 Hz (if 3 channels are used)
Transmission protocol	Bluetooth (Class 1), serial port profile

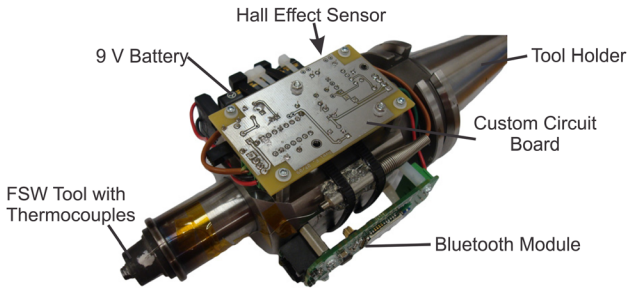

Fig. 4 Photograph of assembled instrumented tool holder for FSW

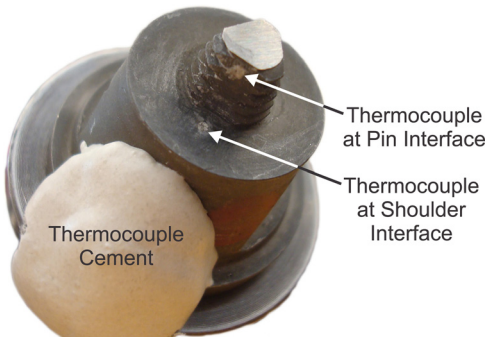

Fig. 5 Close-up view of FSW tool showing the exposed thermocouples at the shoulder-workpiece and pin-workpiece interfaces

4 Experimental Procedure

Welding was performed on a commercial 3-axis computer numerical control (CNC) mill (HAAS TM-1). 175-mm-long butt welds are created between two 203 mm × 102 mm × 4.76 mm (8 in. × 4 in. × 3/16 in.) aluminum 6061-T6 workpieces (unless otherwise noted) at a constant plunge depth of 4.9 mm (position control). The abutting surfaces were milled prior to welding in order to create zero gap butt welds. An FSW tool made of H13 tool steel with a concave shoulder and a threaded, conical pin with three flats is used. The tool shoulder diameter is 15 mm, the pin diameter tapers from 7.0 mm to 5.2 mm and the pin length is 4.7 mm. The tools were machined on a five-axis mill-turn center (Mori Seiki NT1000/W). The tool travel angle was held constant at 3 deg. An 8-mm-thick low carbon steel backing plate is used under the workpieces. As part of a full-factorial series of experiments, the spindle speed is varied from 700 rpm to 1700 rpm in 200 rpm increments (always rotating counterclockwise). For each spindle speed, the travel speed is varied from 100 mm/min to 500 mm/min in 100 mm/min increments, resulting in a total of 29 welds (the weld with 700 rpm and 500 mm/min was not performed to prevent possible damage to the tool due to very low expected temperatures). All samples were orientated so that they were welded parallel to the rolling direction. Welds were also performed at various plunge depths, ranging from 4.6 mm to 5.0 mm in 0.1 mm increments with a constant spindle speed of 1200 rpm and a constant travel speed of 200 mm/min. Although for some welds, the (commanded) plunge depth was higher than the pin length and workpiece thickness (zero plunge depth defined as pin barely in contact with workpiece surface), in these experiments the bottom of the pin was never deep enough to cause pin or backing plate damage (actual plunge depth lower than commanded plunge depth due to machine compliance). Welding parameters were not varied during one weld, i.e., for each parameter combination one full weld with a weld length as indicated above was performed. The welds reached a quasi steady-state during the weld traverse (as can be seen in Fig. 7). The vertical bars in Figs. 6 and 11 indicate the standard deviation of the temperature measurement during the middle 75% of the weld traverse. When averages are reported, they are the mean of the temperature measurement during the middle 75% of the weld traverse. The sampling rate for the (wireless) temperature and angular position measurements is 250 Hz. In addition, welding forces and spindle torque were measured at 2500 Hz using a three-axis force dynamometer (Kistler model 9265 A) and a calibrated current probe, respectively.

5 Results and Discussion

This section demonstrates the efficacy of the developed tool-workpiece interface temperature measurement system during FSW experiments of 6061-T6 aluminum alloy for varying spindle speeds, travel speeds and plunge depths. It is also shown how the temperature measurements provide a better fundamental understanding of the FSW process.

5.1 Average Interface Temperatures. Figure 6 shows the average temperatures experienced at the tool-workpiece interface when varying the spindle speed and travel speed. It can be seen that both the shoulder and pin temperatures increase for higher spindle speeds due to greater heat generation per distance traveled by increased friction and plastic deformation. The temperatures also increase for lower travel speeds due to more heat being deposited per unit weld length. By varying the spindle speed and travel speed in the given tests, the average shoulder temperature varies from 395 °C to 591 °C and the average pin temperature from 389 °C to 580 °C. For all cases tested, the shoulder temperature is greater than or equal to the pin temperature. This is in agreement with the theory that more heat is generated at the tool-shoulder than at the too-pin interface. The measured temperatures approach the solidus temperature of 6061-T6 (582 °C) for higher heat inputs (higher spindle speeds and lower travel speeds) and in a few cases the shoulder temperature is above the solidus temperature, which suggests localized melting at the tool-workpiece interface. Evidence of localized melting has also been reported by Yang et al. [27]. The approach of the average shoulder interface temperature toward the solidus temperature as seen in Fig. 6 supports the self-limiting theory during FSW [28,29], i.e., for higher temperatures, the metal flow stress decreases, resulting in lower spindle torque, reduced friction at the tool-workpiece interface and reduced heat generation. However, Fig. 6 also shows that it is possible to exceed the solidus temperature at the tool-workpiece interface. The data also shows that for the parameter window chosen, varying the spindle speed results in a larger variation in interface temperature than varying the travel speed, which is an important result for developing closed-loop temperature control for FSW.

5.2 Interface Temperature Dynamics. Figure 7 displays the measured interface temperatures of one of the welds performed in this study. It can be seen that the pin temperature rises first, due to the pin contacting the workpiece prior to the shoulder during the tool plunge. While the tool traverses along the joint line, the average temperatures are not increasing significantly (quasi steady-state) and as the tool retracts from the workpiece, the tool temperature cools down.

The temperature measurement approach chosen in this work captures the dynamics of the process very well, because the thermocouple sheaths are in direct contact with the aluminum workpiece at the tool-workpiece interface. The measured temperatures are not constant, but rather oscillating as the tool traverses under constant operating conditions (Fig. 7). The frequency of these oscillations is found to match the frequency of the spindle rotation, i.e., the thermocouple is capturing temperature variations within 360 deg of tool rotation [5]. For the various spindle speeds used in this study and a sample rate of 250 Hz, the system is

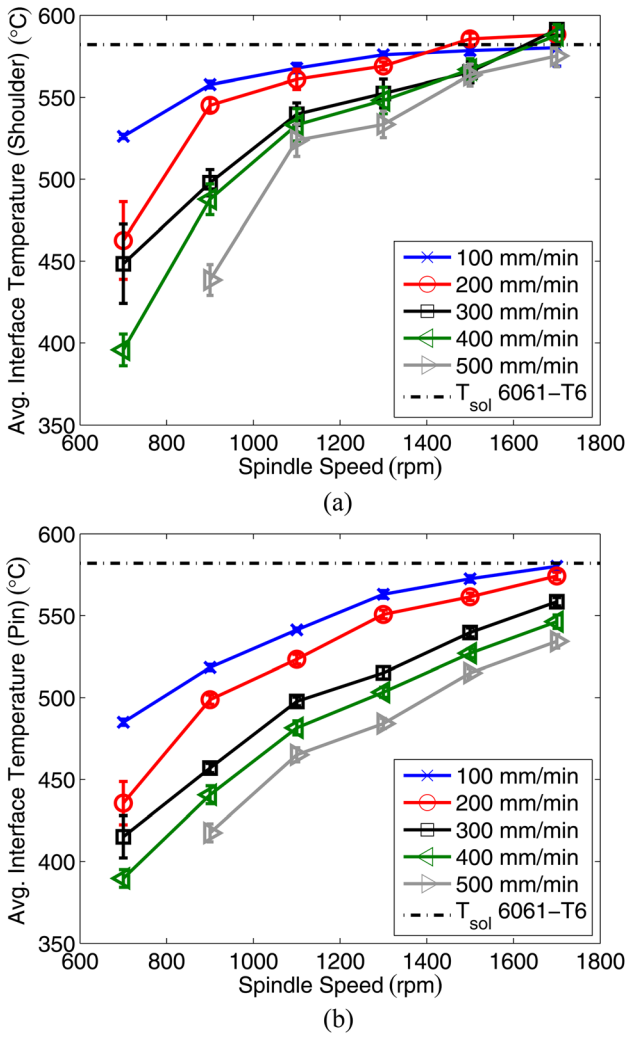

Fig. 6 Average temperatures during weld traverse at (*a*) shoulder and (*b*) pin interface for various spindle speeds and travel speeds for 6061-T6

capturing 8.8–21 temperature measurements per rotation of the tool (angular resolution of 17–41 deg).

There are several potential explanations for the observed interface temperature oscillations. The thermocouple tips are located off centered with respect to the tool rotation axis and in direct contact with the workpiece material. The 3 deg travel angle, the weld traverse motion and the asymmetric nature of FSW (differences between advancing and retreating side) cause a varying temperature field under the tool. A nonzero travel angle can cause uneven pressure distributions under the tool, resulting in differences in heat generation and thus temperature under the shoulder. When the tool is traversing across the workpiece, lower temperatures are experienced ahead of the tool than behind the tool because colder (unwelded) material enters the weld zone ahead of the tool. Both experimental and analytical work reported higher temperatures on the advancing side as compared to the retreating side of the weld due to higher shearing on the advancing side [30–34].

Figure 8 shows the amplitude of the measured interface temperatures at the frequency of the spindle rotation over time (window size of 100 samples, i.e., 0.4 s) using fast Fourier transforms (FFT). It can be seen that the amplitude at the shoulder interface is sharply increasing toward the end of the plunge when the shoulder starts contacting the workpiece (large temperature variations under the tool shoulder solely due to nonzero travel angle). The temperature amplitude then decreases to almost zero during the dwell period of 3 s (material well mixed and hence temperature distribution nearly uniform) and increases again during the weld traverse (temperature differences due to weld traverse and process asymmetry). The temperature amplitude at the pin interface is rather uniform during the plunge, goes to zero during the dwell period and then reaches a value of less than half of the amplitude at the shoulder interface during the weld traverse. The difference between the temperature amplitudes observed at the shoulder and pin interfaces as shown in Fig. 8 is discussed below, taking into consideration a sensor calibration method.

Due to the thermocouple's limited response time and inherent delays due to physical heat conduction as described above, the temperature response is experiencing attenuation in magnitude and a phase lag. A sensor calibration method was developed to correct for this issue and determine the actual tool-workpiece interface's temperature history. Using the thermocouple measurements, the angular position data from the Hall effect sensor and the magnitude and phase information from the sensor calibration, the true temperature distribution under the shoulder and around the pin can be estimated. Both the measured (uncorrected) temperature data and the interface (corrected) temperature data are shown in Fig. 9. Due to the relatively high excitation frequency (i.e., the spindle speed) with respect to the sensor bandwidth, the temperature measurements experience a phase lag and an

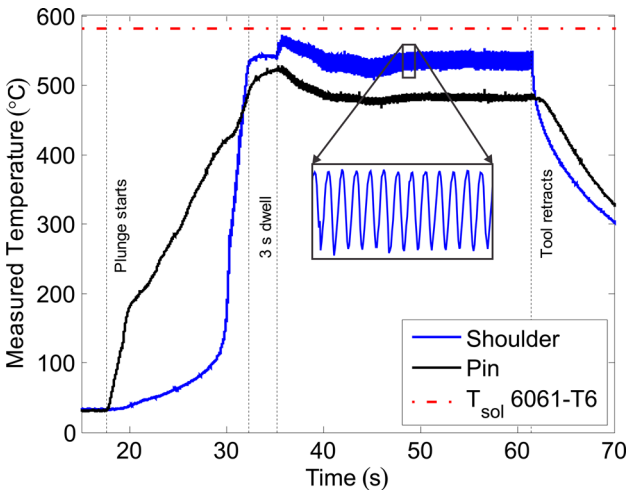

Fig. 7 Measured temperatures for shoulder and pin location during welding of 6061-T6 (solidus temperature 582 °C) at 1100 rpm and 400 mm/min

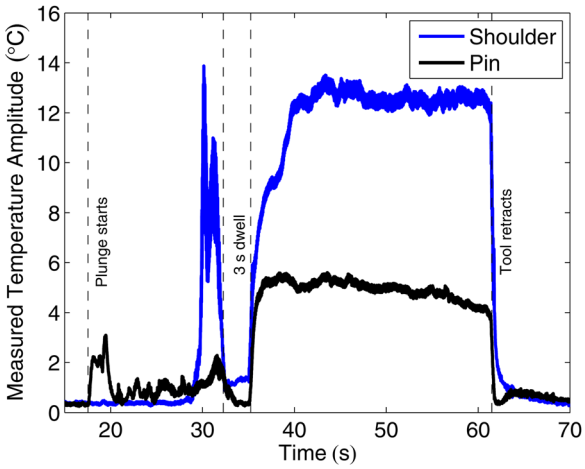

Fig. 8 Measured temperature amplitudes obtained from FFT over time during welding of 6061-T6 at 1100 rpm and 400 mm/min. A moving window of 100 samples (0.4 s or 7.3 tool rotations) was applied.

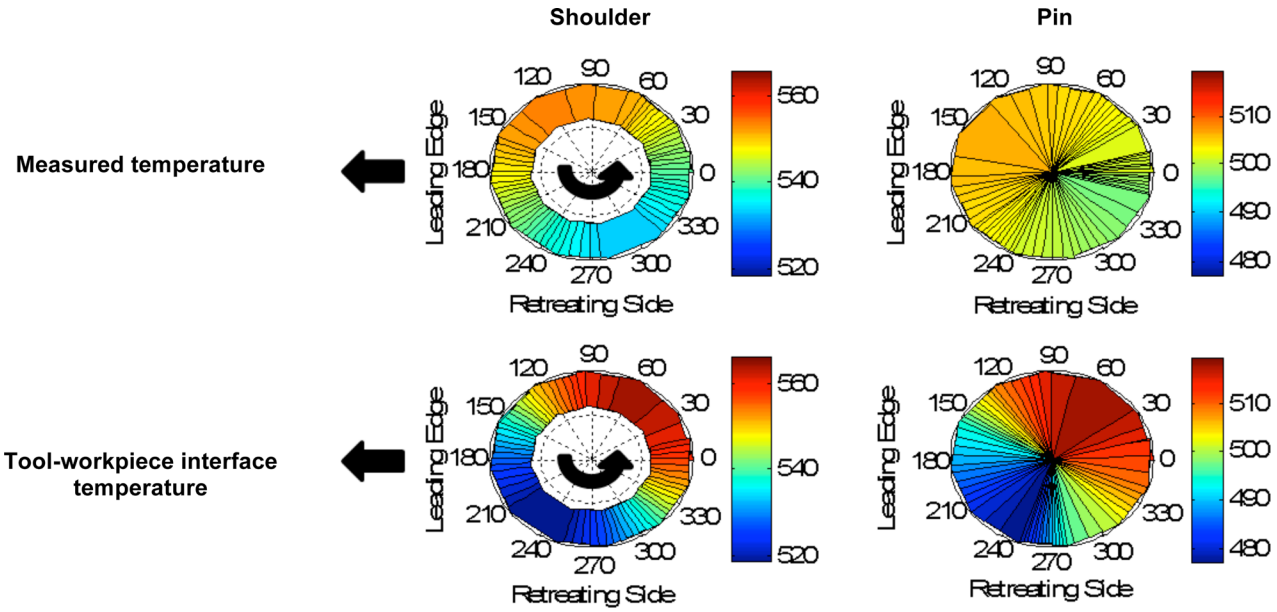

Fig. 9 Measured temperature (°C) and calculated tool-workpiece interface temperature distributions at the shoulder and pin (1300 rpm, 400 mm/min, 6061-T6)

attenuated magnitude. The dynamic measurements are corrected by taking into account the phase lag and the magnitude attenuation from the calibration. The data shows that the differences due to the thermocouple response limitations are significant: for a spindle speed of 1300 rpm, the phase lag at the shoulder is 49 degrees (pin: 91 deg) and the attenuation factor is 0.43 (pin: 0.20). I.e., even though a < 0.25-mm-diameter thermocouple bead was located within 250 μm of the tool surface, the amplitude of the measured temperature oscillations were as small as 20% of the magnitude occurring at the tool-workpiece interface. Using these corrections it was found that the highest temperatures are experienced between the advancing side and the trailing edge of the tool (approximately 60 deg from the trailing edge toward the advancing side as seen in Fig. 9). On the advancing side the velocity gradients are highest, resulting in higher strain rates and more heat generation than on the retreating side. In addition, colder workpiece material coming in from the leading edge (advection heat transfer) is transported further to the retreating side than to the advancing side due to the counterclockwise rotation of the tool and the resulting flow pattern [34]. In Fig. 9 it can be seen that there is a phase difference of approximately 20 deg in the measured (uncorrected) temperature obtained with the sensor at the shoulder versus at the pin location. Since the response characteristics are different for the two sensors (Table 2), the corrected data does not show this phase difference anymore: the time constant for the thermocouple at the shoulder location is shorter.

As seen in Figs. 8 and Fig. 10 for various plunge depths, the as-measured temperature amplitudes are higher at the shoulder interface than at the pin interface. The thermocouple at the shoulder is located further away from the tool rotation axis than the pin thermocouple, thus capturing a larger temperature variation. However, when correcting for the magnitude attenuation based on the developed heat transfer calibration, the temperature amplitude at the pin is higher than at the shoulder interface for the two highest plunge depths (Fig. 10). At the shoulder interface, higher plunge depths result in lower interface temperature amplitudes, i.e., smaller temperature variations between the advancing and retreating side, and leading and trailing edge, hence a more uniform temperature distribution under the shoulder. Low plunge depths result

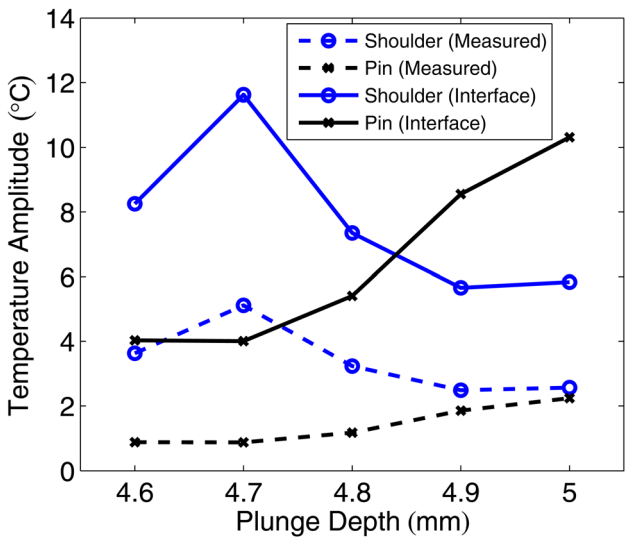

Fig. 10 Amplitudes of measured interface temperature for different plunge depths. Constants: 1200 rpm, 200 mm/min, 6061-T6.

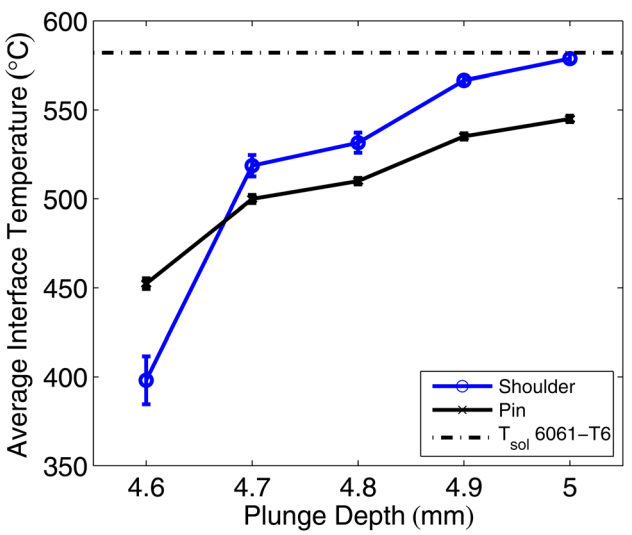

Fig. 11 Average measured interface temperatures for different plunge depths. Constants: 1200 rpm, 200 mm/min, 6061-T6.

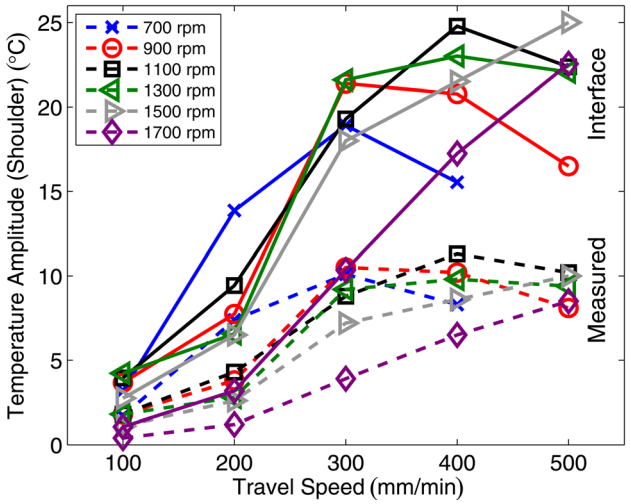

Fig. 12 Amplitudes of interface temperature at shoulder interface during the weld traverse (6061-T6) for various spindle speeds and travel speeds. Plunge depth 4.9 mm (constant).

in insufficient engagement of shoulder and workpiece, especially on the leading edge due to the travel angle, resulting in less heat generation there, causing a larger temperature difference. Higher plunge depths result in a more uniform shoulder engagement on leading and trailing edge, i.e., a smaller temperature difference. At the pin interface, higher plunge depths result in higher interface temperature amplitudes, i.e., higher temperature variations between the advancing and retreating side, and leading and trailing edge, hence a less uniform temperature distribution around the pin. A possible explanation is: for all the plunge depths shown here, the pin is fully engaged into the workpieces, i.e., the major change in average temperature results from the contribution of the shoulder. The thermal diffusivity of the workpieces decreases with increasing temperature [35], caused by higher plunge depths (Fig. 11), which results in less heat removal and a higher temperature difference, i.e., a larger temperature amplitude at the pin interface. The lowest plunge depth (4.6 mm) is a special case, in which there was insufficient contact between shoulder and workpiece, creating an unacceptable weld.

Figures 12 and 13 show how the temperature amplitudes at the shoulder and pin interface, respectively, are strongly dependent on the travel speed and varies between 3 °C and 29 °C (corrected values). Higher travel speeds cause higher advection heat transfer,

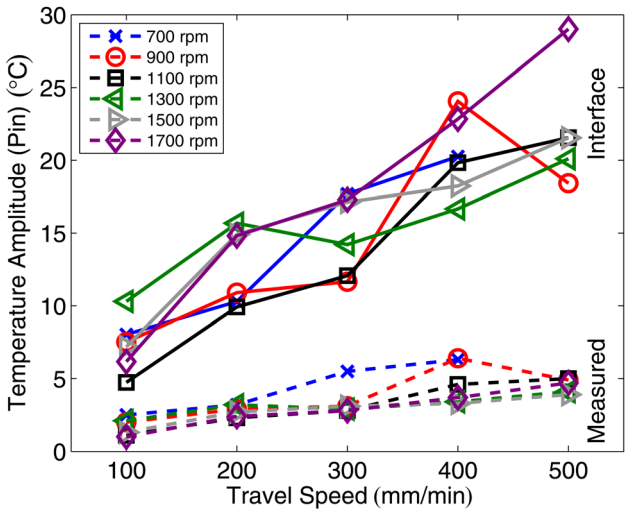

Fig. 13 Amplitudes of interface temperature at pin interface during the weld traverse (6061-T6) for various spindle speeds and travel speeds. Plunge depth 4.9 mm (constant).

and hence a higher asymmetry between advancing and retreating side due to the flow pattern described above. This is reflected in the larger amplitudes being measured. This phenomenon was also observed experimentally and from a numerical model by Simar et al. [32]. The spindle speed does not show any discernable effect on the interface temperature amplitudes.

6 Conclusions

A wireless data acquisition system was built to collect temperature measurements off a rotating tool in a CNC mill during FSW. Two through-holes for placing the thermocouples at the tool-workpiece interface were used for the first time on a seam weld. Using through holes enables the thermocouple sheaths to be in direct contact with the workpiece material. The system captures weld temperature variations (i.e., process dynamics) at the tool-workpiece interface in real-time. Variations of the interface temperature within one rotation of the tool were experimentally observed.

The temperature measurement technique was shown to work reliably over a wide range of operating conditions (various spindle speeds, travel speeds, and plunge depths) for several aluminum alloys and revealed further insight into the process dynamics. The system can be used for process monitoring and detect the occurrence of local melting (exceeding the solidus temperature) at the tool-workpiece interface and hence can limit the degradation of weld quality. Results from this work support the self-limiting theory during FSW, i.e., for higher temperatures, the metal flow stress decreases, resulting in lower spindle torque, reduced friction at the tool-workpiece interface and reduced heat generation. However, temperatures at the shoulder-workpiece interface exceed the solidus temperature for some conditions.

It was demonstrated that based on the relative magnitude of shoulder and pin interface temperatures, welds with insufficient tool shoulder-workpiece contact can be detected, thus potentially identifying and preventing welds with detrimental weld quality due to some forms of lack of penetration (LOP). However, LOP can occur due to a variety of causes, some of which may not relate with tool shoulder-workpiece contact. The temperature distribution underneath the shoulder and around the pin was experimentally measured in great spatial and temporal detail for the first time. It was found that the highest temperatures are at the shoulder interface between the advancing side and the trailing edge of the tool, closer to the advancing side. The temperature distribution was mostly affected by travel speed, also affected by plunge depth but spindle speed showed an insignificant influence (among the tested parameter ranges). The temperature difference within one tool rotation was found to be between 10 °C and 50 °C, depending on the process parameters.

The experimental results from this work have shown to be useful in improving the process understanding and the measurement method can also be a valuable tool to verify thermal models and to establish weld parameters when welding different or dissimilar workpiece materials or geometries by monitoring the interface temperatures. Future work will utilize this temperature measurement technique for the development of improved closed-loop temperature control algorithms to maintain weld quality.

Acknowledgment

Partial support of this work by the Department of Mechanical Engineering and the College of Engineering at the University of Wisconsin—Madison, the Wisconsin Alumni Research Foundation Technology Development RA and the U.S. National Science Foundation under contract CMMI-0824879 is gratefully acknowledged. The Mori Seiki NT1000/W is an equipment loan from the Machine Tool Technology Research Foundation. The authors would like to thank Professor Nicola J. Ferrier, Professor Neil A. Duffie and Mr. Edward G. Cole at the

University of Wisconsin—Madison for their valuable discussions and advice.

Nomenclature

A/D = analog-to-digital converter
CCW = counterclockwise
CNC = computer numerical control
DAQ = data acquisition
EDM = electrical discharge machining
FEM = finite element method
FFT = fast Fourier transform
FSW = friction stir welding
LOP = lack of penetration
T_{sol} = solidus temperature (K)

References

[1] Thomas, W. M., Nicholas, E. D., Needham, J. C., Murch, M. G., Temple-Smith, P., and Dawes, C. J., 1991, "Friction Stir Butt Welding," GB Patent No. 9125978.8.
[2] Mishra, R. S., and Ma, Z. Y., 2005, "Friction Stir Welding and Processing," Mater. Sci. Eng., **R50**, pp. 1–78.
[3] Threadgill, P. L., Leonard, A. J., Shercliff, H. R., and Withers, P. J., 2009, "Friction Stir Welding of Aluminium Alloys," Int. Mater. Rev., **54**(2), pp. 49–93.
[4] Fehrenbacher, A., Cole, E. G., Zinn, M. R., Ferner, N. J., Duffie, N. A., and Pfefferkorn, F. E., 2011, "Towards Process Control of Friction Stir Welding for Different Aluminum Alloys," Friction Stir Welding and Processing VI - Held During the TMS 2011 Annual Meeting and Exhibition, Feb. 27–Mar. 3, Minerals, Metals and Materials Society, San Diego, CA, pp. 381–388.
[5] Fehrenbacher, A., Duffie, N. A., Ferrier, N. J., Pfefferkorn, F. E., and Zinn, M. R., 2011, "Toward Automation of Friction Stir Welding Through Temperature Measurement and Closed-Loop Control," ASME J. Manuf. Sci. Eng., **133**(5), p. 051008.
[6] Perivilli, S., Peddieson, J., and Cui, J., 2008, "Friction Stir Welding Heat Transfer: Quasisteady Modeling and Its Validation," ASME J. Manuf. Sci. Eng., **131**(1), p. 011007.
[7] Smith, C. B., Zinn, M. R., Shultz, E. F., Cole, E. G., Ferrier, N. J., and Pfefferkorn, F. E., 2010, "Effect of Compliance and Travel Angle on Friction Stir Welding With Gaps," ASME J. Manuf. Sci. Eng., **132**(4), p. 041010.
[8] Dehelean, D., Safta, V., Cojocaru, R., Hälker, T., and Ciucă, C., 2008, "Monitoring the Quality of Friction Stir Welded Joints by Infrared Thermography," Proceedings of the IIW 2008 International Conference on Safety and Reliability of Welded Components in Energy and Processing Industry, Graz, Austria, July 10–11, 2008, paper WP4-2, pp. 621–626.
[9] Darras, B. M., Omar, M. A., and Khraisheh, M. K., 2007, "Experimental Thermal Analysis of Friction Stir Processing," Mater. Sci. Forum, **539-543**, pp. 3801–3806.
[10] Burkes, D. E., Hallinan, N. P., Shropshire, K. L., and Wells, P. B., 2008, "Effects of Applied Load on 6061-T6 Aluminum Joined Employing a Novel Friction Bonding Process," Metall. Mater. Trans. A, **39**(12), pp. 2852–2861.
[11] Zettler, R., Potomati, F., Dos Santos, J. F., and De Alcantara, N. G., 2006, "Temperature Evolution and Mechanical Properties of Dissimilar Friction Stir Weldments When Joining AA2024 and AA7075 With an AA6056 Alloy," Welding World, **50**(11–12), pp. 107–116.
[12] Swaminathan, S., Oh-Ishi, K., Zhilyaev, A. P., Fuller, C. B., London, B., Mahoney, M. W., and McNelley, T. R., 2010, "Peak Stir Zone Temperatures During Friction Stir Processing," Metall. Mater. Trans. A, **41**(3), pp. 631–640.
[13] Colegrove, P. A., and Shercliff, H. R., 2003, "Experimental and Numerical Analysis of Aluminium Alloy 7075-T7351 Friction Stir Welds," Sci. Technol. Weld. Joining, **8**(5), pp. 360–368.
[14] Record, J. H., Covington, J. L., Nelson, T. W., Sorensen, C. D., and Webb, B. W., 2007, "A Look at the Statistical Identification of Critical Process Parameters in Friction Stir Welding," Welding J., **86**(4), pp. 97–103.
[15] Cederqvist, L., Garpinger, O., Hagglund, T., and Robertsson, A., 2012, "Cascade Control of the Friction Stir Welding Process to Seal Canisters for Spent Nuclear Fuel," Control Eng. Pract., **20**(1), pp. 35–48.
[16] Shercliff, H. R., and Colegrove, P. A., 2007, "Process Modeling," *Friction Stir Welding and Processing*, R. S. Mishra and M. W. Mahoney, eds., ASM International, Materials Park, OH, pp. 187–217.
[17] Fehrenbacher, A., Pfefferkorn, F. E., Zinn, M. R., Ferrier, N. J., and Duffie, N. A., 2008, "Closed-Loop Control of Temperature in Friction Stir Welding," 7th International Friction Stir Welding Symposium, Awaji Island, Japan, TWI, Published on CD.
[18] McCune, R. W., Murphy, A. A., Price, M. M., and Butterfield, J. J., 2012, "The Influence of Friction Stir Welding Process Idealization on Residual Stress and Distortion Predictions for Future Airframe Assembly Simulations," ASME J. Manuf. Sci. Eng., **134**(3), p. 031011.
[19] Peel, M., Steuwer, A., Preuss, M., and Withers, P. J., 2003, "Microstructure, Mechanical Properties and Residual Stresses as a Function of Welding Speed in Aluminum AA5083 Friction Stir Welds," Acta Mater., **51**, pp. 4791–4801.
[20] Gratecap, F., Racineux, G., and Marya, S., 2008, "A Simple Methodology to Define Conical Tool Geometry and Welding Parameters in Friction Stir Welding," 7th International Friction Stir Welding Symposium, Awaji Island, Japan, TWI, Published on CD.
[21] Simar, A., Brechet, Y., de Meester, B., Denquin, A., and Pardoen, T., 2008, "Microstructure, Local, and Global Mechanical Properties of Friction Stir Welds in Aluminium Alloy 6005A-T6," Mater. Sci. Eng., A, **486**(1–2), pp. 85–95.
[22] Cederqvist, L., Garpinger, O., Hagglund, T., and Robertsson, A., 2012, "Cascade Control of the Friction Stir Welding Process to Seal Canisters for Spent Nuclear Fuel," Control Eng. Pract., **20**(1), pp. 35–48.
[23] Woo, W., Feng, Z., Wang, X. L., Brown, D. W., Clausen, B., An, K., Choo, H., Hubbard, C. R., and David, S. A., 2007, "In Situ Neutron Diffraction Measurements of Temperature and Stresses During Friction Stir Welding of 6061-T6 Aluminium Alloy," Sci. Technol. Weld. Joining, **12**(4), pp. 298–303.
[24] Cederqvist, L., Johansson, R., Robertsson, A., and Bolmsjö, G., 2009, "Faster Temperature Response and Repeatable Power Input to Aid Automatic Control of Friction Stir Welded Copper Canisters," *Friction Stir Welding and Processing*, Vol. 5, R. S. Mishra, M. W. Mahoney, and T. J. Lienert, eds., TMS, Warrendale, PA, pp. 39–43.
[25] Werschmoeller, D., Ehmann, K., and Li, X., 2011, "Tool Embedded Thin Film Microsensors for Monitoring Thermal Phenomena at Tool-Workpiece Interface During Machining," ASME J. Manuf. Sci. Eng., **133**(2), p. 021007.
[26] Gerlich, A., Avramovic-Cingara, G., North, T. H., 2006, "Stir Zone Microstructure and Strain Rate During Al 7075-T6 Friction Stir Spot Welding," Metall. Mater. Trans. A, **37**(9), pp. 2773–2786.
[27] Yang, Y. K., Dong, H., and Kou, S., 2008, "Liquation Tendency and Liquid-Film Formation in Friction Stir Spot Welding," Weld. J. (Miami, FL, U.S.), **87**(8), p. 202s–211s.
[28] Frigaard, Ø., Grong, Ø., Bjørneklett, B., and Midling, O. T., 1999, "Modelling of the Thermal and Microstructure Fields During Friction Stir Welding of Aluminium Alloys," International Friction Stir Welding Symposium, Thousand Oaks, CA, Vol. 1, pp. 1–10.
[29] Tang, W., Guo, X., McClure, J. C., and Murr, L. E. N., 1998, "Heat Input and Temperature Distribution in Friction Stir Welding," J. Mater. Process. Manuf. Sci., **7**(2), pp. 163–172.
[30] Cho, J.-H., Boyce, D. E., and Dawson, P. R., 2005, "Modeling Strain Hardening and Texture Evolution in Friction Stir Welding of Stainless Steel," Mater. Sci. Eng., A, **398**(1–2), pp. 146–163.
[31] Maeda, M., Liu, H., Fujii, H., and Shibayanagi, T., 2005, "Temperature Field in the Vicinity of FSW-Tool During Friction Stir Welding of Aluminium Alloys," Weld. World, **49**(3), pp. 69–75.
[32] Simar, A., Pardoen, T., and de Meester, B., 2007, "Effect of Rotational Material Flow on Temperature Distribution in Friction Stir Welds," Sci. Technol. Weld. Joining, **12**(4), pp. 324–33.
[33] Nandan, R., Roy, G. G., and Debroy, T., 2006, "Numerical Simulation of Three-Dimensional Heat Transfer and Plastic Flow During Friction Stir Welding," Metall. Mater. Trans. A, **37A**(4), pp. 1247–59.
[34] Jacquin, D., De Meester, B., Simar, A., Deloison, D., Montheillet, F., and Desrayaud, C., 2011, "A Simple Eulerian Thermomechanical Modeling of Friction Stir Welding," J. Mater. Process. Technol., **211**(1), pp. 57–65.
[35] Mills, K. C., 2002, *Recommended Values of Thermophysical Properties for Selected Commercial Alloys*, Woodhead Publishing, Cambridge, UK.